

UNIVERSITY OF ZAGREB
FACULTY OF ELECTRICAL ENGINEERING AND COMPUTING

MASTER THESIS num. 1527

From Global to Local: Maintaining Accurate Mobile Manipulator State Estimates Over Long Trajectories

Filip Maric

Zagreb, September 2017.

*Umjesto ove stranice umetnite izvornik Vašeg rada.
Kako biste uklonili ovu stranicu, obrišite naredbu \izvornik.*

dsadsa

CONTENTS

1. Introduction	1
2. Thing mobile manipulator	3
2.1. Ridgeback	4
2.2. UR10	5
2.3. Hokuyo LIDAR	5
2.4. FT300	6
2.5. Robotiq Gripper	6
3. State estimation	7
3.1. State	8
3.2. Kinematic model	9
3.2.1. Forward kinematics	9
3.2.2. Differential forward kinematics	10
3.3. Localization	12
3.3.1. Wheel odometry	12
3.3.2. LIDAR odometry	13
3.3.3. Extended Kalman filter	14
4. Motion planning	15
4.1. Inverse kinematics	15
4.1.1. Differential inverse kinematics	16
4.1.2. The Jacobian pseudoinverse and numerical filtering	16
4.2. Redundancy resolution	17
4.3. Task-priority kinematics	18
4.3.1. Motion planning scheme	18
4.3.2. Drawbacks	19
4.4. Sequential convex optimization	19
4.4.1. Modeling objective and constraint functions	20
4.4.2. Motion planning scheme	22

4.4.3. The SQP algorithm	22
5. Software architecture	24
5.1. Overview	24
5.1.1. Architecture	25
5.2. State estimation	27
5.3. Motion planning	27
5.3.1. Task-priority	27
5.3.2. Sequential convex optimization	27
5.4. Control	28
6. Experimental results	29
6.1. Simulation	29
6.2. Localization	30
6.3. Dual trajectory	32
7. Conclusion	33
Bibliography	34
A. DH parameters	37
B. Robot operating system	39

1. Introduction

In applications ranging from military operations to extraterrestrial exploration, mobile manipulators present themselves as the ideal answer to many challenges being addressed by robots. The mobile platform increases the workspace of a conventional manipulator while also enabling optimal positioning. The increased workspace also provides the capability of performing industrial tasks that would otherwise require multiple manipulators. A comprehensive survey on mobile manipulator systems can be found in (Bloch et al., 2003).

The mobile manipulator can be described as a robotic system composed of a manipulator arm mounted on top of a mobile platform. A variety of issues related to mobile manipulators have been explored in the past two decades. These include dynamic and static stability, force development and application, maximum payload determination, etc. (Papadopoulos and Gonthier, 1999; Korayem and Ghariblu, 2004). However, a majority of the research concerning mobile manipulators deals with motion planning and state estimation (Yamamoto and Yun, 1992; Korayem et al., 2012).

This thesis explores the problems of state estimation and motion planning in the context of an omni-directional mobile manipulator. Chapter 2 introduces the "Thing" mobile manipulator used in this work. Each major component is described in appropriate detail, keeping in mind the context of research presented.

Chapter 3 deals with the challenge of state estimation for a mobile manipulator. Assuming accurate mobile base pose data, it is possible to estimate the state of the manipulator to a reasonable degree of accuracy using only a forward kinematics model described in section 3.2. The primary interest thus lies in obtaining the end effector pose estimate, as other estimates can be derived from it if necessary. Finding the base position relative to the starting position is explored in section 3.3 by fusing local odometry estimates in a probabilistic framework.

Finally, two approaches to motion planning are described in chapter 4. A classical approach enables defining priorities for kinematics tasks assigned to the robot, which are then applied in a classical optimization scheme. The more contemporary *sequential convex optimization* is also explored, which enables defining non-linear inequality and equality constraints. These two approaches offer a powerful framework for local motion planning

and trajectory optimization.

2. Thing mobile manipulator

The Thing mobile manipulator (Figure 2.1) is composed of a Ridgeback omni-directional platform and a UR10 manipulator arm with a Robotiq 3-Finger Adaptive Robot Gripper in place of the end-effector. The three systems are essentially separate on the lower level: the Ridgeback, UR10 and Robotiq gripper local hardware interfaces are electronically independent self-contained systems. These local interfaces are unified by the Ridgeback's computer, which operates as a server under the Robot Operating System (ROS). This interfacing strategy provides all the advantages of distributed computing, such as networked control or information sharing. This platform is also equipped with a vast array of sensors, making it ideal



Figure 2.1: The Thing mobile manipulator

for autonomous robotics research. The Ridgeback platform is outfitted with a Hokuyo laser range finder (LIDAR) and Kinect2 camera , extending both planar and spatial perception capabilities. The omni-directional drive enables field-of-view (FOV) control independent of both end-effector pose and base position, making it an interesting platform for active perception research. The UR10 manipulator is equipped with the FT300 force-torque sensor and an Intel Realsense camera mounted on the gripper, further increasing perception capabilities.

2.1. Ridgeback

The Ridgeback (Figure 2.2) is a midsize indoor robot platform that uses an omni-drive to move manipulators and heavy payloads with minimal constraints. The omnidirectional base provides precision positioning in constrained environments and comes fully integrated with on-board computer, front laser range finder and an IMU. Ridgeback offers native ROS and Gazebo integration and is compatible with a wide range of robot accessories. It is primarily

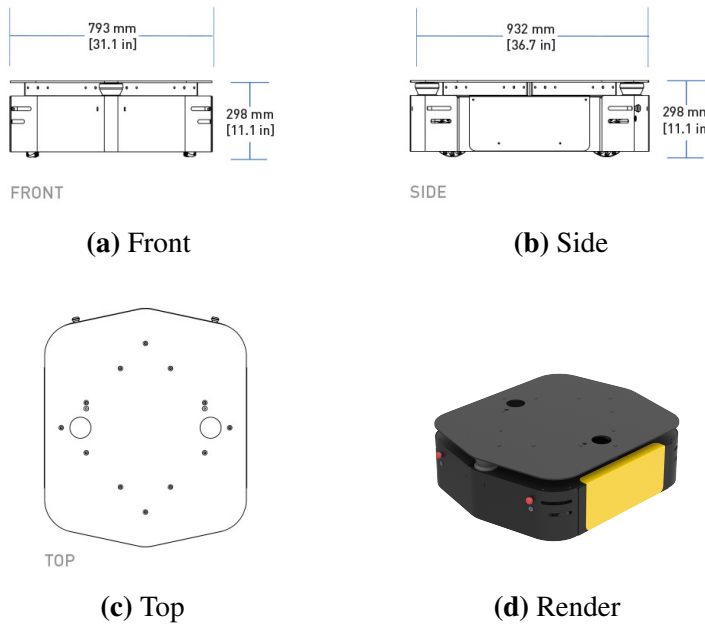


Figure 2.2: The Ridgeback mobile platform

designed for warehousing applications as it is highly flexible in a controlled flat environment. The built in wheel odometry provides accurate local position estimates, with pose drift accumulating very slowly. For improved localization and obstacle avoidance, the navigation stack ROS package provides SLAM capability using the on-board LIDAR and IMU.

In a controlled laboratory setting, this platform enables a high degree of flexibility in research. The high load bearing capability enables the platform to carry manipulators (such as the UR10) and large sensor arrays.

2.2. UR10

The UR10 is Universal Robotics largest collaborative industrial manipulator. It is a full 6DOF robotic arm capable of mimicking human arm movements. During operation it can handle weights up to 10 kg, making it viable for a wide range of tasks. The provided drivers enable performing collaborative tasks alongside human operators, allowing for easy positioning of the arm through compliant movement and preventing use of excessive force on impact.



Figure 2.3: The UR10 manipulator

Weight	28.9 kg
Payload	10 kg
Speed	Large joints: Max 120°/s Wrist joints: Max 180°/s Tool: approx 1 m/s
Repeatability	±0.01 mm
Power	average 350 W

Table 2.1: UR10 specifications

The data in table Figure 2.1 clearly shows that the UR10 manipulator is meant for tasks involving high precision and light payloads. The repeatability value of 0.01 mm shows that the UR10 can reach the same pose multiple times with a high degree of accuracy, which is important in industrial applications. Additionally, it's light weight and high end-effector modularity make it ideal for research purposes.

2.3. Hokuyo LIDAR

The Hokuyo UST-10LX Scanning Laser Rangefinder is a small, accurate, high-speed device for obstacle detection and localization of autonomous robots and automated material handling systems. This model uses Ethernet interface for communication and can obtain measurement data in a wide field of view up to a distance of 10 meters with millimeter resolution. This sensor uses a laser source to scan 270° field of view. Positions of objects in the range are calculated with step angle and distance. Sensor outputs these data through communication channel.



(a) Front

(b) Side

Figure 2.4: The FT300 force-torque sensor

2.4. FT300

The UR10 on the Thing mobile manipulator has a variety of sensors built-in for use in various tasks. One such sensor is the FT300 force-torque sensor by Robotiq. In terms of mechanical fit, the Sensor has an embedded coupling to fit directly on the UR wrist. The tool side of the Sensor matches the UR bolt pattern. Its application range from impedance control to perception and contact calibration of the manipulator.

2.5. Robotiq Gripper



Figure 2.5: The Robotiq gripper

The Robotiq gripper is a three-fingered adaptive gripper used as the end effector on the UR10 manipulator. It is created for applications in advanced manufacturing and robotics research. All the fingers can be independently position, velocity and force controlled and can exert forces from 50 to 60 N at the finger tips.

3. State estimation

State estimation is an often encountered challenge when working with autonomous systems. Most autonomy schemes require accurate information on the current state of the system in order properly modify the system behaviour. This type of system can be generalized as a non-linear system described by a difference equation and observation model with additive noise¹

$$x_k = f(x_{k-1}) + w_{k-1}, \quad x \in \mathbb{R}^n \quad (3.1a)$$

$$z_k = h(x_k) + v_k, \quad z \in \mathbb{R}^k \quad (3.1b)$$

Finding the state estimate \hat{x}_k given the measurements $z_0 \dots z_k$ subject to measurement noise v and past states $x_0 \dots x_{k-1}$ subject to process noise w is the state estimation problem. Various algorithms have been developed using different mathematical frameworks to find the best estimate according to some optimality criterion (Thrun et al. (2005)).



Figure 3.1: The Thing mobile manipulator and the frames subject to estimation

The problem of state estimation for a mobile manipulator is twofold: it is necessary to estimate the state of the end-effector in the local workspace while also placing it in the

¹we leave out separate expressions for input variables as they can be integrated within the functions f and h

global context of a map or starting position. The local state of the end-effector is successfully estimated using a deterministic kinematic model. Joint position values are used to provide a state estimate, ignoring various dynamic and environment effects. Estimating the base state (*localization*) is a more complex problem; the dynamic and environment effects on base movement significantly affect the steady-state. Consequently, in addition to kinematic models we have to rely on movement estimates from sensor data which is inherently noisy. The imperfect model and sensor data are fused in a single estimate using a probabilistic framework.

In this chapter, we first define our state of interest (as seen in Figure 3.1) in section 3.1. Section 3.2 contains details on the derivation of the kinematic model used in end-effector state estimation assuming sufficient knowledge of the base pose. The probabilistic framework used for estimating the base state is described in section 3.3, where wheel and LIDAR odometry are fused to provide an accurate estimate.

3.1. State

Control and task algorithms frequently require information on the pose of the mobile manipulator frames in Cartesian space. A frame pose represents complete information about a frames position and orientation in a given reference frame. The pose is often represented by a *homogenous transformation matrix*

$$T_{k-1}^k = \begin{bmatrix} R & p \\ 0 & 1 \end{bmatrix}. \quad (3.2)$$

The rotation matrix $R \in \mathbb{R}^{3x3}$ represents the orientation of the frame k relative to the frame $k - 1$, while translation is represented by the vector $p \in \mathbb{R}^3$. Estimating the matrix T for the end-effector is a 9-dimensional problem which can be further reduced. It is possible to fully define it the vector r consisting of the translation vector p and a *quaternion* q

$$r_{EE}(T_0^{EE}) = [x \ y \ z \ q_w \ q_x \ q_y \ q_z]^T. \quad (3.3)$$

The number of dimensions can also be reduced for the base, as it moves on a 2D plane and thus only rotates alongside one axis and has a constant z coordinate

$$r_B(T_0^B) = [\hat{x} \ \hat{y} \ \hat{\theta}]^T. \quad (3.4)$$

The estimated state consists of end-effector and base poses comes in the form of a 10-dimensional *task vector* s

$$s = [r_{EE} \ r_B]^T \quad (3.5)$$

Using this representation, the state estimation problem has been reduced from 24 down to 10 dimensions. Reducing the dimensionality of the problem makes it computationally less expensive, which is vital for real-time operation. Considering that the global state estimate in this work is derived exclusively from base odometry data, it is possible to infer the base pose knowing the end-effector pose. However, to maintain generality the formulation in (3.3) and (3.4) is kept.

3.2. Kinematic model

Disregarding the various dynamic and environment effects, the Thing can be modelled as manipulator. The Ridgeback platform is system with holonomic constraints and it's global position and the orientation can be viewed as a chain of two prismatic and a rotational joint. These three joints make up the base upon which we add the kinematic model of the UR10 manipulator. This results in a system kinematically indistinguishable from a redundant manipulator.

The UR10 joint position measurements are reasonably accurate and thus this model can be used to produce a valid local end-effector state estimate. Assuming valid estimates for the base position and orientation, this model will accurately represent the global state of the mobile manipulator.

3.2.1. Forward kinematics

Forward kinematics are defined as a set of equations that express the pose of a certain frame on a kinematic chain as a function of configuration-space values

$$q = \begin{bmatrix} q_0 & q_1 & q_2 & q_3 & q_4 & q_5 & \hat{x} & \hat{y} & \hat{\theta} \end{bmatrix}^T . \quad (3.6)$$

The equations are commonly derived using the transforms defined in (3.2). The transform between two frames can be defined as a function of only four parameters using the Denavit-Hartenberg notation (Uicker et al., 1964).

$$T_{k-1}^k(d, \theta, a, \alpha) = \begin{bmatrix} \cos \theta_k & -\cos \alpha_k \sin \theta_k & \sin \alpha_k \sin \theta_k & a_k \cos \theta_k \\ \sin \theta_k & \cos \alpha_k \cos \theta_k & -\sin \alpha_k \cos \theta_k & a_k \sin \theta_k \\ 0 & \sin \alpha_k & \cos \alpha_k & d_k \\ 0 & 0 & 0 & 1 \end{bmatrix} . \quad (3.7)$$

The parameters a, α are usually constant and represent the structure, while d, θ represent the prismatic and rotational joint values and biases. Using the DH parameters as defined in Table A.1, we derive all the transforms (3.7) from global frame to the end effector frame.

Multiplying these transforms gives us the transform from the global frame to any frame of the mobile manipulator

$$T_0^{EE} = \prod_{k=1}^{N_{EE}} T_{k-1}^k . \quad (3.8)$$

The forward kinematics model is subject to various joint angle and link length biases, as it is possible the given DH parameters do not exactly correspond to the physical manipulator. However, the estimate provided has a significantly lower error than that of base localization and thus can be disregarded in the current analysis.

It is also interesting to note that the forward kinematics equations are non-injective surjective functions: every q corresponds to a single pose T , even though a given T might correspond to multiple or infinite values of q . The analytic formulation of the transform from the global frame to the end-effector can be found in the appendix.

3.2.2. Differential forward kinematics

Equations defined in subsection 3.2.1 provide an estimate of the mobile manipulator state (3.5) using the configuration vector q . However, algorithms used in motion planning and trajectory optimization require an estimate on how configuration change affects the state. This information is contained within the manipulator Jacobian J . We define the Jacobian J as the derivative of the function $f(x) : \mathbb{R}^n \rightarrow \mathbb{R}^k$ with respect to the vector x .

$$J = \begin{bmatrix} \frac{\partial f_1}{\partial x_1} & \frac{\partial f_1}{\partial x_2} & \cdots & \frac{\partial f_1}{\partial x_n} \\ \frac{\partial f_2}{\partial x_1} & \frac{\partial f_2}{\partial x_2} & \cdots & \frac{\partial f_2}{\partial x_n} \\ \vdots & & & \\ \frac{\partial f_k}{\partial x_1} & \frac{\partial f_k}{\partial x_2} & \cdots & \frac{\partial f_k}{\partial x_n} \end{bmatrix} . \quad (3.9)$$

Now \dot{f} can be calculated by multiplying the matrix with \dot{x}

$$\dot{f} = J\dot{x} . \quad (3.10)$$

For a sufficiently small Δ , (3.10) can be extended to produce a first order approximation \hat{f}_k

$$\hat{f}_k = f_{k-1} + J(x_k - x_{k-1}) . \quad (3.11)$$

This framework can be employed in various state estimation and motion planning algorithms.

End-effector Jacobian

For motion planning applications, an estimate on how configuration change affects the end-effector pose Δr_{EE} is vital. The end-effector Jacobian is defined as the derivative of the end-effector pose (3.3) with respect to the configuration vector q . While it can be derived analytically, it is often advantageous to derive it using the geometry of the chain. Here the Jacobian takes the form

$$J = \begin{bmatrix} J_v \\ J_\omega \end{bmatrix}, \quad (3.12)$$

where the matrix J_v is the position Jacobian and J_ω matrix is the orientation Jacobian. In this case, the components representing orientation change are equal to the rotation axes of the joint q_j

$$J_{\omega_j} = \frac{\partial o}{\partial q_j} = z_j. \quad (3.13)$$

The components representing position difference for rotational joints are

$$J_{v_j} = \frac{\partial p}{\partial q_j} = z_j \times (w - p_j). \quad (3.14)$$

For prismatic joints the orientation component is $J_{\omega_j} = 0$, while the translational component lies on the z axis

$$J_{v_j} = \frac{\partial p}{\partial q_j} = z_j. \quad (3.15)$$

As seen in algorithm 1, the geometric derivation is suitable for software implementation as it does not require symbolic calculations and relies only on matrix operations. The *twist* vector w is defined as the composition of translational and rotational velocities. For a sufficiently small pose difference Δr , the vectors are approximately equal

$$w = \begin{bmatrix} v \\ \omega \end{bmatrix} \approx \begin{bmatrix} \Delta p \\ \Delta o \end{bmatrix} = \Delta r. \quad (3.16)$$

Calculating the position difference is straightforward and comes down to subtracting the goal and current positions

$$\Delta p = p - p_{goal}. \quad (3.17)$$

The orientation difference is calculated as follows (Sciavicco and Siciliano, 2012)

$$\Delta o = 0.5L^{-1}(n_c \times n_d + s_c \times s_d + a_c \times a_d), \quad (3.18a)$$

$$L = -0.5([n_c]_x [n_d]_x + [s_c]_x [s_d]_x + [a_c]_x [a_d]_x). \quad (3.18b)$$

Plainly stated, this is the equivalent of angular velocity defined by two different orientations.

Algorithm 1: Geometric Jacobian calculation

Data: Kinematic chain transforms T_i and joint type flags rev_i

Result: End-effector Jacobian matrix J

```
1  $T = I;$ 
2 for  $i = 1, 2, \dots, N$  do
3    $T = TT_i;$                                 /* get next transform */
4    $R_i = R(T);$ 
5    $O_i = O(T);$ 
6   if  $i = 1$  then /* element corresponding to the base joint */
7      $z_i = (rev_i)\mathbf{1};$ 
8      $v_i = (rev_i)z_i \times w + (1 - rev_i)z_i;$ 
9   else /* all subsequent joints */           /*
10     $z_i = (rev_i)R_{i-1} \begin{bmatrix} 0 & 0 & 1 \end{bmatrix}^T;$ 
11     $v_i = (rev_i)z_i \times (r - O_{i-1}) + (1 - rev_i)z_i;$ 
12  end
13 end
14  $J = \begin{bmatrix} v & z \end{bmatrix}^T;$           /* compose the Jacobian */
```

3.3. Localization

When using the kinematic model in section 3.2 sufficiently accurate base pose estimates $\hat{x}, \hat{y}, \hat{\theta}$ are assumed. In reality, obtaining accurate pose estimates is non-trivial and often requires fusing sensor data while taking in to account the probabilistic nature of measurements.

Localization of the Thing mobile manipulator employs a motion model of the omnidirectional drive on the Ridgeback and data provided by the LIDAR. The wheel and LIDAR odometry provide Cartesian velocity estimates with covariance data. This data is fused using an extended Kalman filter and the resulting estimate is more accurate (in theory) than simply integrating wheel odometry data.

3.3.1. Wheel odometry

In classical mechanics a system may be defined as *holonomic* if all constraints of the system are holonomic. For a constraint to be holonomic it must be expressible as a function:

$$f(x_1, x_2, x_3, \dots, x_N, t) = 0 \quad (3.19)$$

i.e. a holonomic constraint depends only on the coordinates x_j and time t . It does not depend on the velocities or any higher order derivative with respect to time t . Decoupled

translational and angular velocities make the estimation process less prone to error, as angular velocities are usually much more difficult to estimate. Having wheel encoder velocity readings w_0, w_1, w_2, w_3 , a base twist estimate $\hat{\xi}$ can be calculated

$$\hat{\xi} = \frac{R}{4} \begin{bmatrix} 1 & 1 & 1 & 1 \\ -1 & 1 & -1 & 1 \\ -\frac{1}{k} & -\frac{1}{k} & \frac{1}{k} & \frac{1}{k} \end{bmatrix} \begin{bmatrix} w_0 \\ w_1 \\ w_2 \\ w_3 \end{bmatrix}. \quad (3.20)$$

Integrating the velocities from (3.20) makes it possible to localize the base relative to the starting position. Odometry estimates are assumed to have a normal distribution, accounting for measurement noise and kinematic nature of the model that ignores dynamic effects.

$$\xi \sim \mathcal{N}(\mu_\xi, \Sigma). \quad (3.21)$$

The covariance matrix Σ in (3.21) is set to a constant value empirically found to sufficiently represent estimate uncertainty

$$\Sigma = \text{diag}(0.001, 0.001, 0.001, 100000, 100000, 0.03). \quad (3.22)$$

3.3.2. LIDAR odometry

A velocity estimate can also be obtained using The Hokuyo LIDAR presents itself as a rich source of information on the environment which can be used to estimate base velocity. Various algorithms exist that implement LIDAR odometry, they are mostly based on Iterative Closest Point matching (ICP) (Besl et al., 1992). In this work we use the a range flow-based approach available in the form of the `rf2o_laser_odometry` ROS package.

While this work does not cover the details of this algorithm, the formulation is relatively straightforward. Given a base twist ξ , for every point sensed by the LIDAR a geometric residual $\rho(\xi)$ is defined

$$\begin{aligned} \rho(\xi) = & R_t + (x \sin \theta - y \cos \theta - R_\alpha k_\alpha) \omega + \left(\cos \theta + \frac{R_\alpha k_\alpha \sin \alpha}{r} \right) v_x \\ & + \left(\sin \theta + \frac{R_\alpha k_\alpha \cos \alpha}{r} \right) v_y. \end{aligned} \quad (3.23)$$

To obtain an accurate estimate, the sensor motion is computed by minimizing all geometric residuals within the cost function F :

$$F(\rho) = \frac{k^2}{2} \ln \left(1 + \left(\frac{\rho}{k} \right)^2 \right), \quad (3.24)$$

$$\hat{\xi} = \min_{\xi} \sum_{i=1}^N F(\rho_i(\xi)). \quad (3.25)$$

Details on parameters and minimization procedure can be found in (Jaimez et al., 2016).

3.3.3. Extended Kalman filter

The wheel and LIDAR odometry data is fused using an Extended Kalman Filter ² (Fujii, 2013). A process and observation model is used to represent the movement of the Thing mobile manipulator:

$$x_k = f(x_{k-1}) + w_{k-1}, \quad x \in \mathbb{R}^n, \quad (3.26a)$$

$$z_k = h(x_k) + v_k, \quad z \in \mathbb{R}^k. \quad (3.26b)$$

Without going in to detail on the derivation of the EKF algorithm, it can be described as having two steps. the model forecast step uses the motion model and last estimated state \hat{x}_k^+ to produce an *a priori* estimate of the next state \hat{x}_k^- and covariance P_k^-

$$\hat{x}_k^- = f(\hat{x}_{k-1}^+) \quad (3.27a)$$

$$P_k^- = J_f(\hat{x}_{k-1}^+) P_{k-1}^+ J_f^T(\hat{x}_{k-1}^+) + Q_{k-1} \quad (3.27b)$$

The correction step makes use of local sensor odometry to calculate the *Kalman gain* K_k and produce *a posteriori* estimates \hat{x}_k^+ and P_k^+

$$\hat{x}_k^+ \approx \hat{x}_k^- + K_k(z_k - h(\hat{x}_k^-)) \quad (3.28a)$$

$$P_k^+ = (I - K_k J_h(\hat{x}_k^-)) P_k^- \quad (3.28b)$$

$$K_k = P_k^- J_h^T(\hat{x}_k^-) (J_h(\hat{x}_k^-) P_k^- J_h^T(\hat{x}_k^-) + R_k)^{-1} \quad (3.28c)$$

The J_f and J_h matrices in (3.27) (3.28) represent the process and measurement model Jacobians, while the process and measurement noise covariance is represented by the Q and R matrices. Estimates provided by (3.27) (3.28) are first-order estimates, higher order estimators of this type exist but are computationally infeasible for real-time applications.

It is also important to note that the EKF assumes white Gaussian noise and thus can only be successfully applied when the actual process and measurement noise have a near-Gaussian distribution.

²EKF in rest of text

4. Motion planning

As mentioned in chapter 3, the primary motion planning objective consists of reaching the desired pose with the end-effector and mobile base. However, moving the mobile manipulator safely and efficiently in the workspace is more involved and significantly constrains the primary objective. For instance, it is important to maintain distance from obstacles both with the platform and the manipulator. Additionally, various other performance metrics exist which may need to be maximized or maintained above a certain value. These objectives and constraints can be formalized in a way that fits the motion planning problem.

In section 4.1 the *inverse kinematics* problem is considered for mobile manipulator. This involves finding an configuration q that corresponds to a given end-effector pose r . Section 4.2 explores the problem of utilizing the extra degrees of freedom of the system to optimize movement, also referred to as *redundancy resolution*. The remaining sections explore two different approaches to redundancy resolution: *task-priority* and *sequential convex optimization*. The classic task-priority algorithm is computationally efficient extension to the optimization approach for inverse kinematics, but also highlights the drawbacks of a purely linear optimization algorithm. A more contemporary approach of sequential convex optimization provides a more general and powerful optimization infrastructure that is highly modular, at the cost of computational efficiency.

4.1. Inverse kinematics

Regulating kinematic tasks that are configuration dependent reduces to the problem

$$f(q) = 0. \quad (4.1)$$

where $q \in \mathbb{R}^n$ is the configuration vector. The classical approach to inverse kinematics would have us find the inverse of the function f

$$q = f^{-1}(0). \quad (4.2)$$

However, this inverse can only exist in non-redundant configurations, otherwise the number of solutions is infinite. Even in cases where the configuration is non-redundant , the

inverse function is still occasionally impossible to derive. In order to solve this problem, an optimization approach which avoids dealing with complicated analytical expressions is employed.

4.1.1. Differential inverse kinematics

In an inverse differential kinematics scheme used for redundant kinematic chains, $f(q)$ is regulated to the target value using

$$\frac{\partial}{\partial q} f = -\lambda_f f(q), \lambda_f > 0. \quad (4.3)$$

The solution to (4.3) is often rank-deficient, so a least squares formulation is employed

$$\min_{\dot{q}} \frac{1}{2} \left\| \frac{\partial f}{\partial q} \dot{q} + \lambda_f f(q) \right\|^2, \lambda_f > 0. \quad (4.4)$$

Letting $J = \frac{\partial f}{\partial q}$ and $a = -\lambda_f f(q)$, the solution to (4.4) that minimizes the L_2 norm is given by finding the pseudoinverse of the A matrix

$$\dot{q} = J^\dagger a. \quad (4.5)$$

4.1.2. The Jacobian pseudoinverse and numerical filtering

In (4.3)-(4.17), the pseudoinverse operation denoted by \dagger is defined as

$$J^\dagger = J^T (JJ^T)^{-1}. \quad (4.6)$$

While more numerically stable than the classic inverse operator in (4.2), this method is also subject to *kinematic singularities* in the manipulator. These are configurations where the linear system requires a large configuration change in order to accomplish a given task space change. The components of the task Jacobian $\frac{\partial f}{\partial q}$ then approach 0, resulting in loss of rank. Implementing the pseudo-inverse in a numerically stable way is very important for robustness and non-trivial.

Damped pseudoinverse

We often use the more numerically stable *damped pseudoinverse* (Chan and Lawrence, 1988)

$$J^\# = J^T (JJ^T + \lambda I)^{-1}, \lambda \in \mathbb{R}. \quad (4.7)$$

There are also various contemporary approaches to implementing the pseudoinverse (Chiaverini et al., 1994). In this work we use the *selectively damped pseudoinverse* (Buss and Kim, 2005), alongside with *singular value filtering* described in (Colomé and Torras, 2015).

Selectively damped pseudoinverse

The matrix pseudoinverse operation can be performed using an SVD decomposition of the Jacobian

$$J = \sum_i \sigma_i u_i v_i^T, \quad (4.8)$$

$$J^T (JJ^T)^{-1} = \sum_i \frac{1}{\sigma_i} v_i u_i^T. \quad (4.9)$$

The pseudoinverse would in this case have the form

$$J^T (JJ^T + \lambda I)^{-1} = \sum_i \frac{\sigma_i}{\sigma_i^2 + \lambda} v_i u_i^T, \quad (4.10)$$

this *selectively damped pseudoinverse* (Buss and Kim, 2005) equates to choosing a specific value λ_i for each singular value σ_i

$$J^\# = \sum_i \frac{\sigma_i}{\sigma_i^2 + \lambda_i} v_i u_i^T. \quad (4.11)$$

Singular value filtering

The singular values of a Jacobian determine its stability with respect to inversion. Lower singular values indicate that the matrix is closer to being singular. A proposed approach to solving this problem prior to using a specific inversion technique is *singular value filtering* (Colomé and Torras, 2012). This technique sets the lowest singular value of a given jacobian matrix J to σ_0

$$h_{v,\sigma_0}(\sigma) = \frac{\sigma^3 + v\sigma^2 + 2\sigma + 2\sigma_0}{\sigma^2 + v\sigma + 2}. \quad (4.12)$$

In (4.12) the shape factor v determines the difference between modified and original singular values $h_{v,\sigma_0}(\sigma) - \sigma$, a higher v results in lower differences. This results in a new Jacobian matrix

$$\hat{J} = \sum_i h_{v,\sigma_0}(\sigma_i) u_i v_i^T. \quad (4.13)$$

Authors report that combining this filtering method with any of the above pseudoinverse approaches results in higher stability.

4.2. Redundancy resolution

Given that the valid set of solutions to (4.4) is in an affine subspace $\mathcal{F} \in \mathbb{R}^n$, the minimization scheme for solving a lower priority set of tasks would be

$$\min_{\dot{q} \in \mathcal{F}} \frac{1}{2} \left\| \frac{\partial g}{\partial q} \dot{q} + \lambda_g f(q) \right\|^2, \lambda_g > 0. \quad (4.14)$$

The process of defining additional constraints for a redundant system, thus reducing the affine subspace \mathcal{F} is called *redundancy resolution*. The general solution to (4.14), which minimizes the L_2 norm of the primary task while making redundant DOFs available to other inputs z has the form

$$\dot{q} = J^\# a + (I - J^\# J) z, z \in \mathbb{R}^n. \quad (4.15)$$

The operator $(I - J^\# J)$ is an orthogonal projector, thus the effect of the control z will not affect the outcome in a way that cancels out the first term.

4.3. Task-priority kinematics

In (Nakamura et al., 1987; Nakamura, 1990), *null-space optimization* is utilized to achieve execution of a secondary task B given a primary task A

$$\dot{q} = A^\dagger a + (I - A^\dagger A) \tilde{B}^\dagger (b - BA^\dagger a) + (I - A^\dagger A) (I - \tilde{B}^\dagger \tilde{B}) z, \quad (4.16a)$$

$$\tilde{B} = B (I - A^\dagger A). \quad (4.16b)$$

This **task-priority** approach to inverse kinematics can be extended to any number of tasks (Slotine, 1991). The main weakness of task-priority lies in the fact that lower-priority tasks will often become infeasible, causing the occurrence of an *algorithmic singularity* (Bailieul, 1985). In (Chiaverini, 1997), a modified approach is introduced , which guarantees robustness

$$\dot{q} = A^\dagger a + (I - A^\dagger A) B^\dagger b + \left(I - \begin{pmatrix} A \\ B \end{pmatrix}^\dagger \begin{pmatrix} A \\ B \end{pmatrix} \right) z. \quad (4.17)$$

Here the trade-off is lower accuracy and slower convergence because the expression is only an approximation of (4.16a).

4.3.1. Motion planning scheme

The motion planning scheme implemented using the task priority formulation is focused on simplicity and robustness rather than optimal movement. The primary task is reaching a goal pose with the end effector, which is vital for most mobile manipulator applications. The secondary task handles mobile base trajectory following. As mentioned in section 4.3, this framework can be extended to any number of tasks, but the increasing numerical instability results in diminishing returns.

$$\Delta q \approx J_{EE}^\dagger \Delta r_{EE} + (I - J_{EE}^\dagger J_{EE}) J_B^\dagger \Delta r_B. \quad (4.18)$$

4.3.2. Drawbacks

The main drawback to task-priority kinematics in (4.16a) and (4.17) is that they cannot natively handle nonlinear inequality constraints (Moe et al., 2016) and equality constraints. Having the ability to define this type of constraint in motion planning is important for more complex systems such as mobile manipulators.

There are currently no open-source implementations for task-priority schemes , as the parameters and structure of the scheme vary greatly depending on the tasks and kinematic chain structure. A more general definition of the problem as a non-linear constrained optimization problem would allow us to utilize the vast array of open-source solvers, implementations and solution schemes developed for a wider range of problems.

4.4. Sequential convex optimization

Performing tasks with a kinematic chain can also be formulated as a bounded non-linear optimization problem P . The non-linear objective function f is minimized subject to non-linear inequality and equality constraints g, h , while keeping the parameter vector x within bounds.

$$\begin{aligned} \min_x \quad & f(x) \\ \text{s.t. } & x \in [x_{\min}, x_{\max}] \\ & g(x) \leq C_g \\ & h(x) = C_h \end{aligned} \tag{4.19}$$

We can solve this problem iteratively, by repeatedly constructing and minimizing a convex approximation of the problem \tilde{P} until constraints are satisfied. With \tilde{f} being the quadratic approximation of the objective function f ,

$$\tilde{f}(x) = f(x^k) + \nabla f(x^k)(x - x^k) + \frac{1}{2}(x - x^k)^T H f(x^k)(x - x^k). \tag{4.20}$$

and \tilde{g}, \tilde{h} being local affine approximations of constraint functions

$$\begin{aligned} \tilde{g}(x) &= g(x^k) + \nabla g(x^k)(x - x^k), \\ \tilde{h}(x) &= h(x^k) + \nabla h(x^k)(x - x^k). \end{aligned} \tag{4.21}$$

Using quadratic programming (QP) techniques, we solve \tilde{P}

$$\begin{aligned} \min_x \quad & \mathcal{L}(x, \mu) \\ \text{s.t. } & x \in [x_{\min}, x_{\max}] . \end{aligned} \tag{4.22}$$

Where $\mathcal{L}(x, \mu)$ represents the problem Lagrangian

$$\mathcal{L}(x, \mu) = \tilde{f}(x) + \mu \sum_{i=1}^{i_{\max}} \tilde{g}_i(x) + \mu \sum_{j=1}^{j_{\max}} \tilde{h}_j(x). \tag{4.23}$$

The Lagrange multiplier $\mu > 0 \in \mathbb{R}$ is a large positive value that regulates the priority of constraints over the objective function. Setting a sufficiently large value for μ turns the problem into a constraint satisfaction problem

$$\mathcal{L}(x, \mu) \approx \sum_{i=1}^{i_{max}} \tilde{g}_i(x) + \sum_{j=1}^{j_{max}} \tilde{h}_j(x), \quad (4.24)$$

ignoring main objective function minimization in lieu of satisfying constraints.

4.4.1. Modeling objective and constraint functions

The objective function $f(x)$ can include various terms relating to kinematic and dynamic behaviour of the kinematic chain. An important thing to keep in mind is that these constraints

Minimizing state change

In kinematic planning $f(x)$ is often employed to keep the chain in a configuration close to the seed configuration x_{seed}

$$f(x) = (x - x_{seed}) W (x - x_{seed})^T. \quad (4.25)$$

This results in more predictable solutions to the problem, often avoiding non-modelled dynamic constraints resulting from large changes in configuration.

Pose control

We regulate the execution of a pose goal r using equality constraint functions of the type

$$\Delta r = 0. \quad (4.26)$$

Convexifying (4.26) results in the familiar linear equation

$$h(x) = |J(x - x_k) - \Delta r| = 0. \quad (4.27)$$

In the case of a Cartesian task-space, the error between target pose and current pose in (4.27) can be represented in the form of a 6D vector

$$\Delta r = \log(T_{target}^{-1}(a) T_{current}(x)). \quad (4.28)$$

The log operator here is the matrix log operator. This vector can also be obtained using identities (3.18).

Obstacle avoidance

Obstacle avoidance can be handled as an inequality constraint in the NL optimization problem. The simplest way of implementing this is using the constraint function

$$g(x) = |p_{base} - p_{obstacle}| \leq Rq, . \quad (4.29)$$

This can in turn be extended to any number of obstacles. Collision checking libraries are often used to find a set of closest points for which to optimize.

Manipulability maximization

Having a metric M that describes the distance from singularity of the system Jacobian, we could use the scheme in (4.19) to optimize task execution. The manipulability metric of a kinematic chain has a couple of different definitions, the one used here is

$$M = \sqrt{\det(JJ^T)}. \quad (4.30)$$

Here J is the kinematic chains Jacobian with respect to the Cartesian (although not necessarily) task-space. Through matrix manipulation it is possible to obtain a closed-form expression for the manipulability Jacobian

$$\frac{\partial M}{\partial x} = \frac{1}{2\sqrt{\det(JJ^T)}} Tr \left((JJ^T)^{-1} \frac{\partial (JJ^T)}{\partial x} \right). \quad (4.31)$$

It might be possible to get this expression in symbolic form, but can be inefficient for real-time applications. Even though maximizing the manipulability measures increases the product of singular values, it does not mean that the smallest singular value will be sufficiently large. Another metric which minimizes size difference between singular values is the *condition number* κ

$$\kappa = \frac{\sigma}{\sigma_0}. \quad (4.32)$$

This value will ideally be close to 1, which means all the singular values are roughly the same magnitude. However this does not maximize the magnitude of singular values itself. The objective function to maximize a combination of these two metrics

$$f(x) = \sqrt{\frac{\kappa}{M}}. \quad (4.33)$$

In the context of the mobile manipulator following both an end effector and base trajectory, this means that the optimization will utilize the mobile base orientation θ to maximize manipulability while ensuring that all the singular values are roughly the same magnitude.

4.4.2. Motion planning scheme

The full motion planning scheme can now be presented as an non-linear optimization problem. The parameter vector is in the case the configuration vector of the mobile manipulator as defined in (3.6)

$$\begin{aligned} \min_q \quad & \sqrt{\frac{\kappa}{M}} \\ \text{s.t.} \quad & \Delta r_{EE} = 0, \\ & (q_x - x_{goal})^2 + (q_y - y_{goal})^2 \leq R^2, \\ & q_{arm} \in [q_{min}, q_{max}], \\ & q_\theta \in [-\theta, +\theta]. \end{aligned} \tag{4.34}$$

The objective function is the modified manipulability metric from (4.33), minimizing this function drives the manipulator away from singular configuration. The end-effector pose trajectory is introduced as a convex constraint function, alongside with the base position and orientation tolerances used for optimization. Additionally, we limit the search space to within the joint limits $[q_{min}, q_{max}]$.

4.4.3. The SQP algorithm

Sequential convex optimization optimization can be tackled using sequential quadratic programming (SQP) (Schulman et al., 2013; Xu et al., 2010), a powerful algorithm which repeatedly constructs and minimizes a convex approximation of the problem \tilde{P} until constraints are satisfied.

Initialize The cost and constraint functions can be picked at runtime or compile time. An advantage of picking the functions at runtime lies in having the ability to parametrized generic versions of commonly used constraints such as collision avoidance or field of view maintenance.

Convexify For each point in the desired trajectory and the penalty value μ , we form convex cost and constraint functions at the operating point. The cost function is convexified to a second-order approximation while the constraints are linearized at the current configuration.

Minimize The convexified problems are minimized, where the parameter values being considered are subject to the trust region δ . This prevents the minimization process from taking large steps when the changes in the convex cost and constraint models do not reflect the changes in the non-linear models to a sufficient degree.

Trust Region At each iteration of the innermost for loop, a trust region δ for the QP problem is updated depending on how well the change proposed by the minimization algorithm translates to the change in non-linear models of the cost and constraint functions. If the change is deemed sufficient, the step size for the next iteration is increased by modifying the parameter search area of the optimization algorithm.

Check constraints Once the convexify loop converges (the changes in q become sufficiently small) or reaches a maximum number of iterations, the result is checked against constraints. If the constraints are satisfied, the algorithm concludes. Otherwise, the penalty μ is increased (usually by a degree of magnitude) and the algorithm is repeated.

Algorithm 2: The SQP algorithm

Data: q_{init}

Result: Configuration q satisfying f, g, h

```

1  $f, g, h \leftarrow \text{Initialize}();$                                 /* Initialize problem */
2 for  $\text{PenaltyIteration} = 1, 2, \dots$  do
3   for  $\text{ConvexifyIteration} = 1, 2, \dots$  do
4      $\tilde{f}, \tilde{g}, \tilde{h} \leftarrow \text{Convexify}(f, g, h);$           /* convexify problem */
5     for  $\text{TrustRegionIteration} = 1, 2, \dots$  do
6        $\min_q G(\tilde{f}, \tilde{g}, \tilde{h})$ ;                                /* minimize */
7       s.t.  $q \in [q - \delta, q + \delta]$ 
8       if  $\text{TrueImprove} / \text{ModelImprove} \geq c$  then
9          $\delta \leftarrow \tau^+ \delta;$       /* expand trust region and proceed */
10        break;
11      end
12       $\delta \leftarrow \tau^- \delta;$           /* shrink trust region and repeat */
13    end
14    if  $\text{Converged}()$  then
15      break;
16    end
17    if  $\text{SatisfiesConstraints}$  then /* Check nonlinear constraints */
18      return  $q;$ 
19    else
20       $\mu = k * \mu;$ 
21    end
22 end

```

5. Software architecture

With the theoretical framework for state estimation and motion planning established in chapter 3 and chapter 4, this chapter describes the software implementation of these ideas. Developing code that is intuitively structured is key in a research context, where it is often maintained and expanded by multiple parties. Maintaining a heavily tested core code-base which allows modular drop-in components for high level functions is an optimal development strategy for such cases. Such a structure expedites testing and data gathering procedures, as it enables quick start-up, user safety and damage prevention.

In section 5.1 development considerations are explained in more detail and a high-level overview of the software architecture is presented. Next, in section 5.2 and section 5.3 state estimation and motion planning pipelines are presented in more detail. Lastly, section 5.4 describes the control pipeline that relays user commands to the API and internal control loops.

5.1. Overview

Developing software for a complex system such as the Thing mobile manipulator is a time-consuming process, as each change requires extensive testing before it can be applied safely. Aside from maintaining a strict version control strategy with tools such as *git*, the developer needs to have an idea of what interaction a given change can have with the rest of the code-base as it is often inefficient to test every change in detail. Structuring the code in a way that decouples most of the heavily-tested core functionalities from specific user tasks is of great importance since it helps the developer maintain an idea of what certain changes can affect.

The testing procedure on the real robot suffers from a high set-up cost, which can be reduced by having start-up procedures stored in the form of ROS launch files. Having a simulation that reasonably models the robots behaviour also expedites testing, as some concepts remain largely unaffected by dynamic effects occurring in reality. Furthermore, platform-agnostic code is maintained, meaning that the software does not differentiate between the simulated and real systems, drastically reducing implementation time.

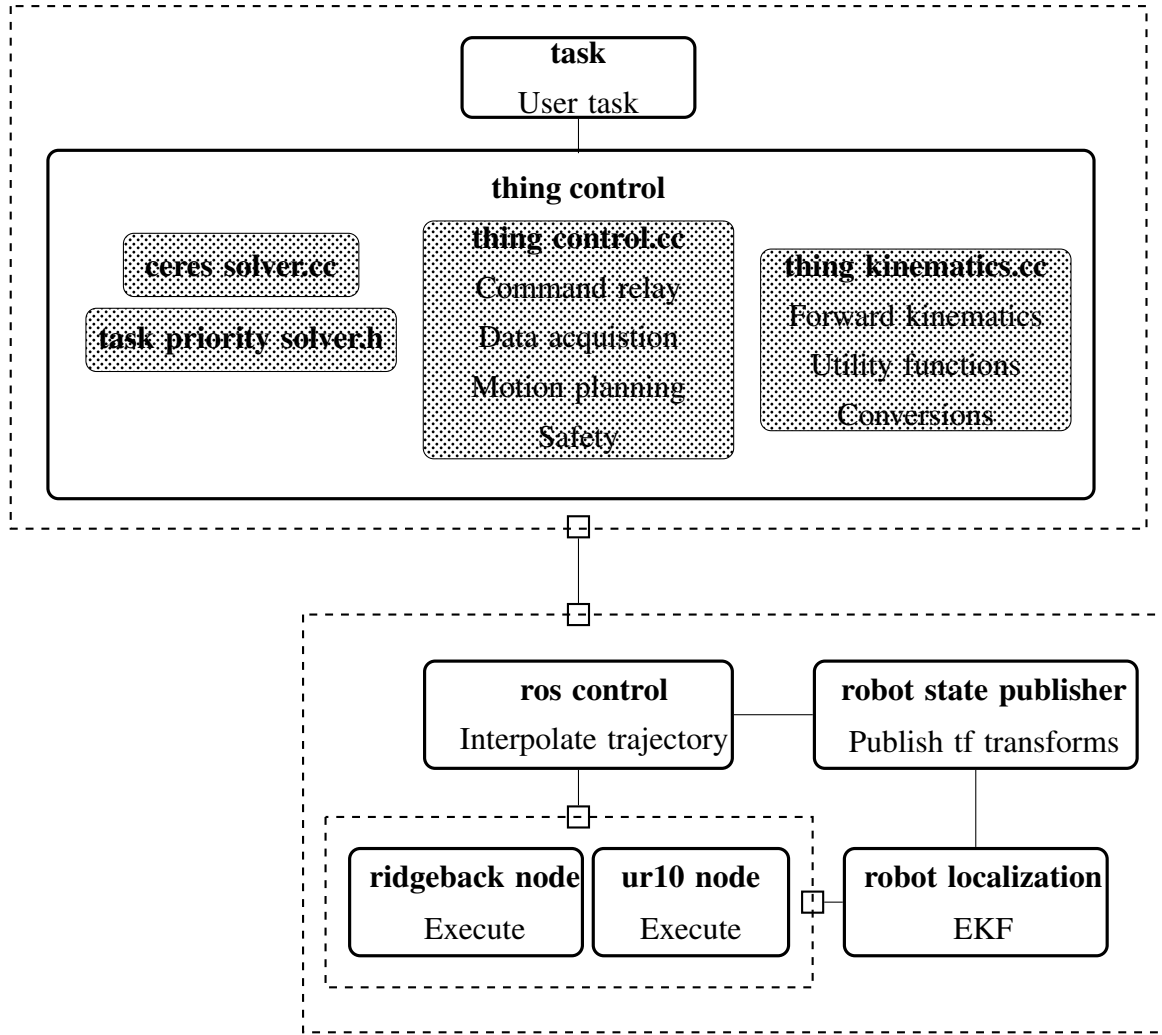


Figure 5.1: Overview of the software architecture. White rounded rectangles represent ROS packages, while cross-hatched rectangles represent individual libraries/headers/executables.

5.1.1. Architecture

The network-based nature of ROS systems allows a distributed software architecture. This enables keeping real-time dependent functionalities on the robot while running high level algorithms on a separate machine. Specifically, the control algorithms implemented in `ros_control` interface with the local UR10 and Ridgeback drivers and are ran on the robot's local machine which acts as a server. Task-specific programs are ran on a separate machine or client which connects to the Thing's ROS core via WiFi or ethernet.

Client

Figure 5.1 shows how the `thing_control` package forms a robust core of the code-base. It acts as a central node which processes trajectories and commands sent by the user, which includes:

- Receiving and processing data streams from the robot
- Sending joint-level commands to the lower-level control architecture
- Processing (solving) Cartesian trajectories sent by the user
- Monitoring incoming data streams and implementing security procedures

Receiving and sending data is done through the ROS topic interface; subscribers fetch structured data from network locations called topics which are populated using publishers.

At compile time, the user can choose a motion planner developed specifically for the Thing mobile manipulator. These planners inherit from a core part of the code-base, the `thing_kinematics` library. This library contains the common mathematical framework for the motion planners as well as various useful kinematics functions:

- Forward kinematics and Jacobian functions
- Pose error calculations
- Angle representation conversions
- Various matrix operations

Keeping this part of code in library form allows for easy transfer of these useful functionalities to other packages. The motion planners (also referred to as *solvers*) represent different approaches to the problem of solving a given Cartesian trajectory. Both the methods presented in section 4.3, section 4.4 are implemented as motion planning libraries.

Server

The computer located on the robot itself or server maintains the control and estimation pipeline on the robot and takes care of publishing the current state and status to the network.

Direct communication with the base and manipulator is achieved through their respective APIs, but in order to connect these libraries to our networked software structure the `ros_control` package is used. It provides a valuable set of tools that abstract the notion of a robot interface and enable quick and easy integration of APIs into ROS-based system architectures.

The transforms representing all of the chains located in the robots URDF¹ file resulting from state estimation are published through the `robot_state_publisher` package. The package publishes the transforms in the form of standardized `\tf` ROS messages. The package is launched on the robot's local machine since the standardized structure of the control pipeline relies on the transforms published by this package.

¹*Unified Robot Description Format* - Standard file format used for semantic robot descriptions.

5.2. State estimation

The EKF algorithm described in section 3.3 is available as a component of the `robot_localization` package (Moore and Stouch, 2014). This package fuses odometry estimates provided by various sources, ideally resulting in a higher-accuracy estimate. The estimates need to be published to a ROS topic in the form of a `nav_msgs/odometry` message. Each state estimation node in `robot_localization` begins estimating the vehicle's state as soon as it receives a single measurement. If there is a holiday in the sensor data (i.e., a long period in which no data is received), the filter will continue to estimate the robot's state via an internal motion model.

5.3. Motion planning

Two motion planning algorithm have been developed, one implementing the *task-priority* (section 4.3) scheme and the other implementing the scheme in (4.34) via the SQP (section 4.4) algorithm.

Unifying the implementations is a common linear algebra framework, the Eigen² library. The Eigen3 library is a powerful linear algebra toolbox capable of handling a vast array of dense and sparse matrix calculations. It is also templated and heavily optimized for reducing redundant value copying and memory management, making it the basis of many algorithm implementations across a range of fields.

5.3.1. Task-priority

Unlike the SQP implementations, task-priority is implemented using only the Eigen3 and C++ standard libraries. It relies on *singular value filtering* (4.12) and the *selectively damped least squares* (4.11) formulation to maintain numeric stability in the pseudoinverse operation. These functions have been developed from scratch in highly abstracted template form for the purposes of this work and are publicly available.

5.3.2. Sequential convex optimization

Implementation of the sequential convex optimization algorithm is done using Google Ceres³ solver as the underlying convex optimization subprogram. The objective and convexified constraint functions are implemented as classes in order to be compatible with the solver.

²http://eigen.tuxfamily.org/index.php?title=Main_Page

³<http://ceres-solver.org/>

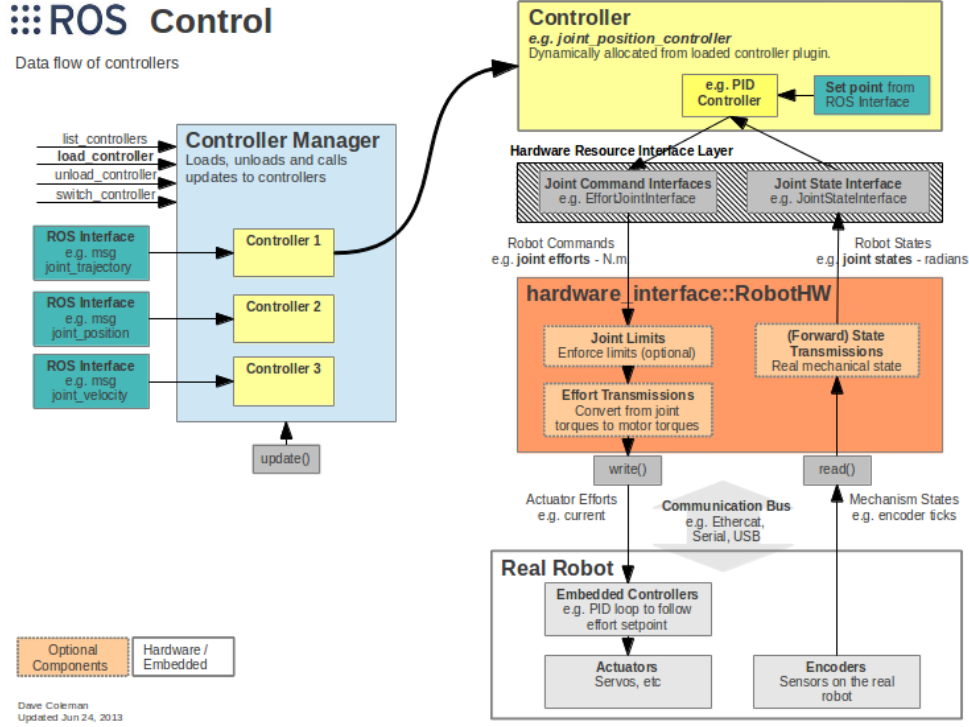


Figure 5.2: Scheme of ros_control functionalities

Ceres is configured to run using the Levenberg–Marquardt trust-region strategy with the Broyden–Fletcher–Goldfarb–Shanno algorithm being used for performing line search.

5.4. Control

The underlying control architecture of the Thing mobile manipulator relies heavily on the internal APIs of both the UR10 and Ridgeback. Thus, the main challenge in implementing the software architecture lies integration of control inputs and outputs rather than parametrization of a control loop. The `ros_control` package functions as an integration tool for robot APIs into the networked structure of ROS-based systems. The `hardware_interface` (Figure 5.2) class is used to wrap the read and write methods of the respective APIs in to function handles. These handles can then be used by a selection of controllers within the package to either forward commands or implement a control loop. A ros controller has many types and is configured using a yaml file. Depending on the interface, this controller will forward commands or actually control the signal using tunable PID parameters. Additionally, we use the joint trajectory controllers which can handle and interpolate multiple timed trajectory points.

6. Experimental results

This chapter covers the results of the presented state estimation and motion planning approaches. Since motion planning was considered on a purely kinematic level, it is extensively tested in both simulation and on the real robot. State estimation testing proved more difficult as dynamic effects such as slip are not easily simulated. For this reason state estimation was only explored in data sets collected from the real robot. Localization tests were performed in



(a) Tests in the VICON laboratory

(b) Simulation testing setup

Figure 6.1: Example of some real and simulated test setups.

the VICON laboratory at the University of Toronto Institute for Aerospace Studies (UTIAS). VICON is a commercial motion capture system ideal for the purposes of setting ground-truth values for state estimation tests and is used as such in all of the tests in this chapter.

6.1. Simulation

The Thing mobile manipulator is simulated using the Gazebo simulator. Aside from being open-source, the main advantage of this simulator is that it is fully integrated within the ROS ecosystem. Furthermore, the `ros_control` controllers used on the actual robot are also integrated in the Gazebo simulation, expediting the implementation procedure.

6.2. Localization

Figure 6.2 shows the results of base localization on a dataset consisting of manual Ridgeback movement inputs. Two variants are compared: the first variant uses an EKF to achieve fusion of both the wheel and LIDAR odometry, the second variant integrates wheel odometry alone using the EKF only to account for measurement noise. Ground truth was established using the VICON¹ motion capture system, which provides sub-millimetre level accuracy.

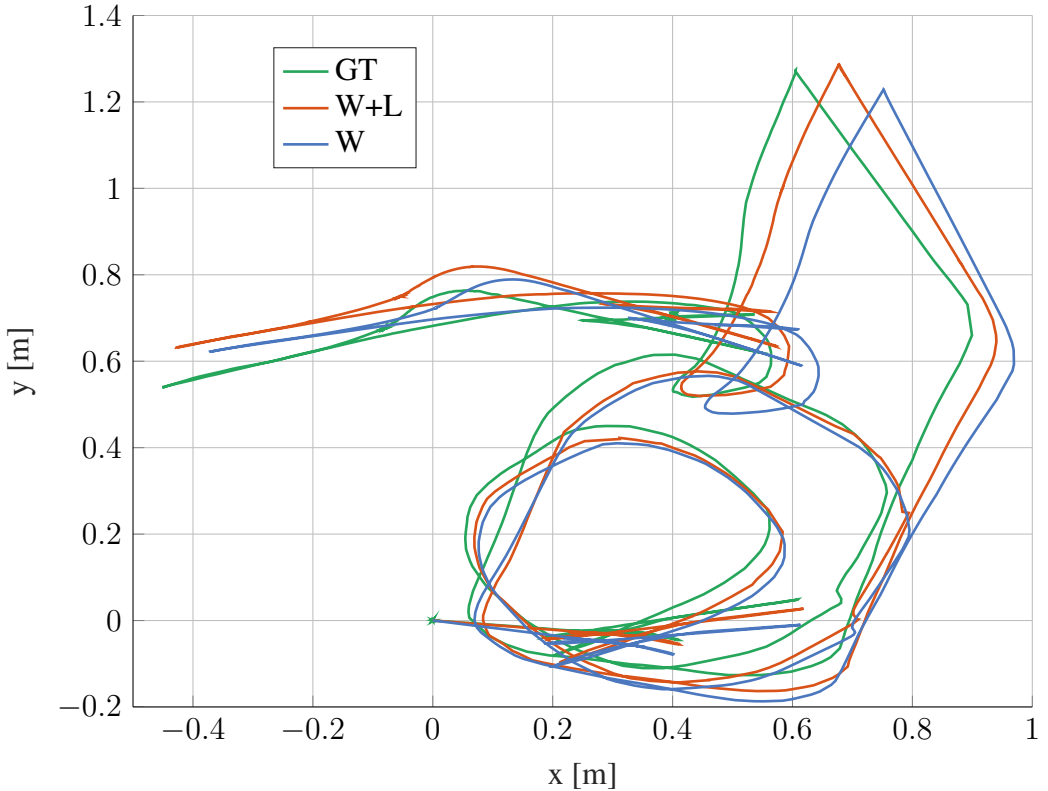


Figure 6.2: Localization using a fusion of wheel and LIDAR odometry (W+L) to the wheel odometry alone (W). The ground truth (GT) is established using the VICON motion capture system.

The expected result would show that fusing two odometry sources provides a better motion estimate than using wheel odometry alone. However, this might not always be the case as the LIDAR odometry algorithm from subsection 3.3.2 relies heavily on the number of data points. Additionally, the LIDAR odometry algorithm provides a covariance matrix that is associated with the coarse-to-fine scheme of the solver and not the uncertainty of the pose estimate itself. This is seen in 6.3, where the mean squared error (MSE) of the base pose estimates is shown. The position MSE of the fused odometry is a slight improvement over the wheel odometry alone, however this depends on the orientation of the vehicle and the number of obstacles the LIDAR is facing. Looking at the orientation MSE, it is visible that

¹<https://www.vicon.com/>

the fused estimate actually becomes worse than the alternative, which should never happen with an EKF if proper covariances are provided.

In absolute terms , both methods have an increasing MSE that is reasonably low. After 120 seconds of fast erratic movement, the position MSE of 0.05 [m]^2 equates to about 20 [cm] of error. It is the authors opinion that this shows advantages of an holonomic omni-drive over the standard wheeled drives, as a high degree of robustness is shown both in angle and position estimates. A global position estimate source such as a GPS could periodically improve the base position estimate, compensating for the odometry error.

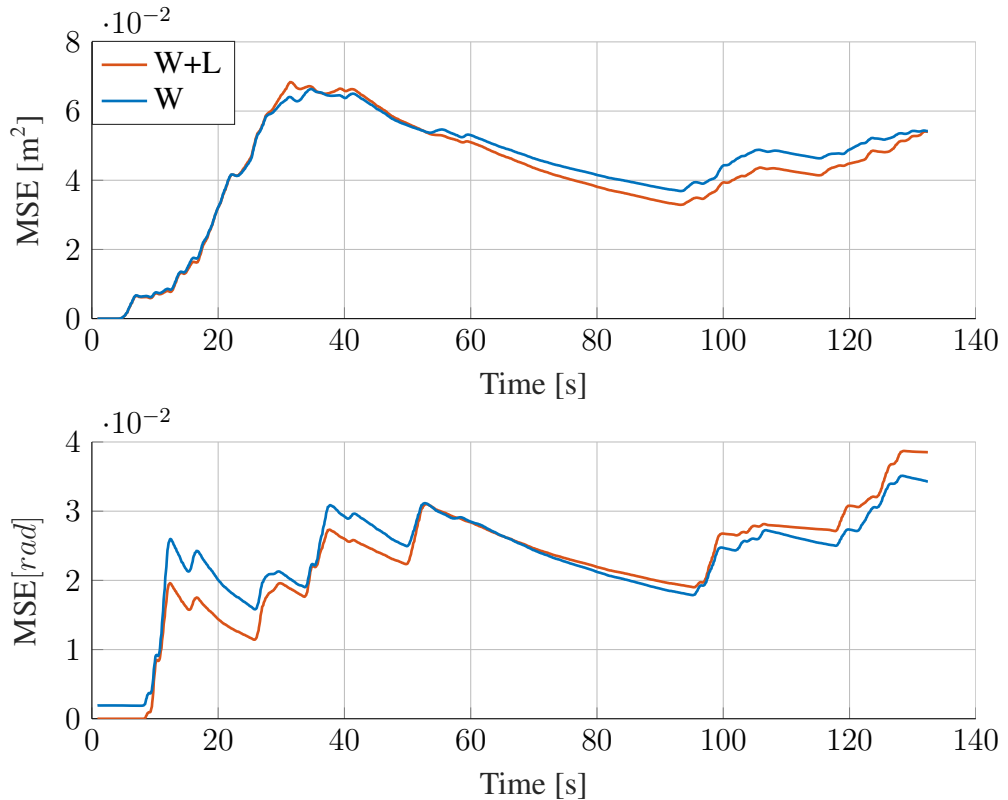


Figure 6.3: The mean squared error of the position (**top**) and orientation (**bottom**) estimates.

The conclusion drawn is that further tuning of the covariance matrix for the LDIAR odometry is necessary. Another option would be using an algorithm based on ICP, where a closed-form formulation for covariance is available (Censi, 2007). Further improvements to localization could also be obtained by using more sensors. The Ridgebacks IMU sensor was not available for this work due to hardware problems. It stands to reason that it would improve the estimate, especially since the wheel odometry + IMU pairing is ubiquitous in mobile robot state estimation problem

6.3. Dual trajectory

As a final test, a dataset of the mobile manipulator performing a 2 metre long trajectory was collected. The goal trajectory involves the Ridgeback following a sinusoidal reference while the arm draws a straight line with constant orientation. The choice of trajectory was made based on prospective mobile manipulator tasks such as welding or spray painting.

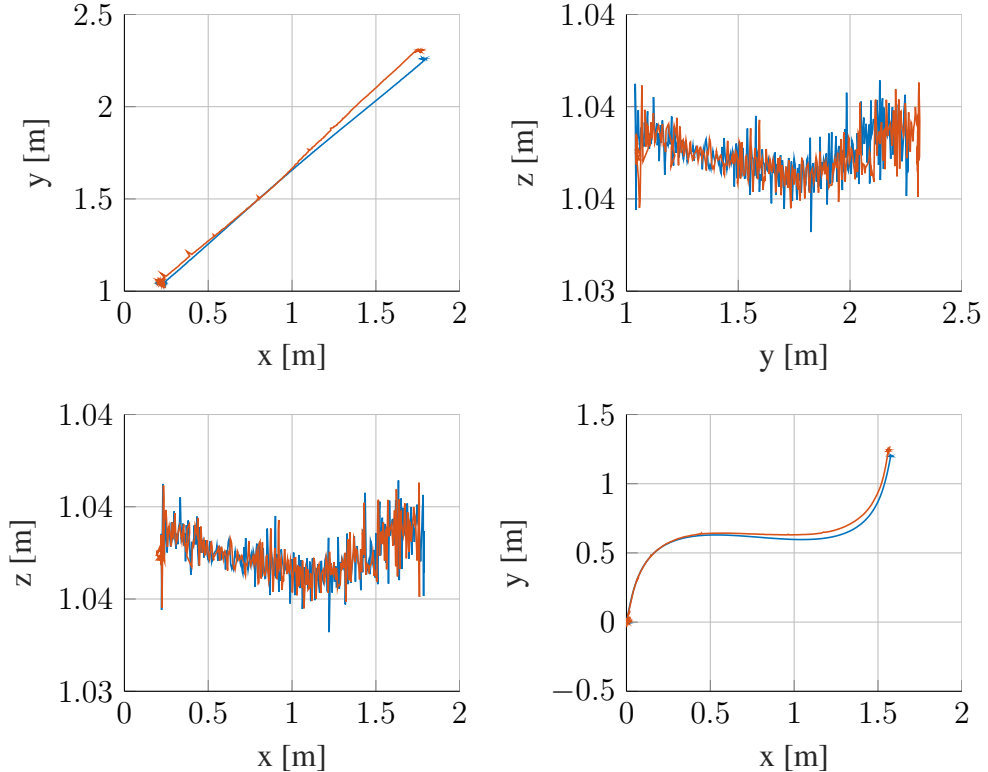


Figure 6.4: The positions of mobile manipulator frames during trajectory execution, comparison of ground truth and estimate. The lower right corner shows the Ridgeback trajectory, while the other three plots shows the end-effector trajectory from different viewpoints.

From 6.4 it can be concluded that the end-effector and base estimate deviation from the ground truth is heavily correlated. Moreover, both frames significantly deviate in the x-y (ground) plane. The estimation error in the bottom left and top right plots showing the y-z and x-z planes is negligible. From this, the assumption made in 3 is confirmed. More precisely, this means that the majority of the end-effector state estimation error stems from localization.

The trajectory joint solution is driven to an arbitrary error using the motion planning scheme. Errors still emerge from the fact that the control is purely kinematic and thus ignores dynamic effects. For this reason the scheme presented in this work is vulnerable to non-controlled environments.

7. Conclusion

In this thesis an analysis of a full motion planning and state estimation solution for a mobile manipulator was presented. It has been found that the majority of state estimation errors stem from base localization. The state estimation solution utilizes the wheel and laser range finder odometry fused using an extended Kalman filter to provide a reasonable base pose estimate.

Two motion planning methods which solve for a base and end-effector trajectory are successfully implemented. A classical task priority approach is used as a tried-and-true approach while sequential convex optimization is presented as a more contemporary approach which enables advanced trajectory optimization. Trajectory optimization methods have been explored which leverage the omni-directional nature of the base, opening up the possibility of various kinematic and active perception solutions.

A software architecture is developed for interfacing with user defined Cartesian trajectories. An approach is taken which defines an robust and highly tested core for interfacing with the local controllers, taking motion planning solutions as modules which can in turn be developed separately. Individual software components are ran in ROS scheme, enabling networked interfacing which is in itself highly tested and modular.

The results show successful performance of long Cartesian trajectories, subject to a decrease of position estimate accuracy with time. A manipulability optimization scheme is tested in simulation, showing promising results. Future work can be done on several different aspects. The motion planning scheme could be modified in an intelligent manner using AI methods, changing trajectory optimization criteria depending on the environment. Other avenues would include improving the state estimates using SLAM or more odometry sources, utilizing the gripper for tasks, or performing sensor calibration autonomously.

BIBLIOGRAPHY

- John Baillieul. Kinematic programming alternatives for redundant manipulators. In *Robotics and Automation. Proceedings. 1985 IEEE International Conference on*, volume 2, pages 722–728. IEEE, 1985.
- Paul J Besl, Neil D McKay, et al. A method for registration of 3-d shapes. *IEEE Transactions on pattern analysis and machine intelligence*, 14(2):239–256, 1992.
- Anthony Bloch, John Baillieul, Peter Crouch, Jerrold E Marsden, Dmitry Zenkov, Perinkulam Sambamurthy Krishnaprasad, and Richard M Murray. *Nonholonomic mechanics and control*, volume 24. Springer, 2003.
- Samuel R Buss and Jin-Su Kim. Selectively damped least squares for inverse kinematics. *Journal of Graphics tools*, 10(3):37–49, 2005.
- Andrea Censi. An accurate closed-form estimate of icp’s covariance. In *Robotics and Automation, 2007 IEEE International Conference on*, pages 3167–3172. IEEE, 2007.
- Stephen K Chan and Peter D Lawrence. General inverse kinematics with the error damped pseudoinverse. In *Robotics and Automation, 1988. Proceedings., 1988 IEEE International Conference on*, pages 834–839. IEEE, 1988.
- Stefano Chiaverini. Singularity-robust task-priority redundancy resolution for real-time kinematic control of robot manipulators. *IEEE Transactions on Robotics and Automation*, 13(3):398–410, 1997.
- Stefano Chiaverini, Bruno Siciliano, and Olav Egeland. Review of the damped least-squares inverse kinematics with experiments on an industrial robot manipulator. *IEEE Transactions on control systems technology*, 2(2):123–134, 1994.
- Adria Colomé and Carme Torras. Redundant inverse kinematics: Experimental comparative review and two enhancements. In *Intelligent Robots and Systems (IROS), 2012 IEEE/RSJ International Conference on*, pages 5333–5340. IEEE, 2012.

Adria Colomé and Carme Torras. Closed-loop inverse kinematics for redundant robots: Comparative assessment and two enhancements. *IEEE/ASME Transactions on Mechatronics*, 20(2):944–955, 2015.

Keisuke Fujii. Extended kalman filter. *Refernce Manual*, 2013.

Mariano Jaimez, Javier G Monroy, and Javier Gonzalez-Jimenez. Planar odometry from a radial laser scanner. a range flow-based approach. In *Robotics and Automation (ICRA), 2016 IEEE International Conference on*, pages 4479–4485. IEEE, 2016.

Moharam Habibnejad Korayem and H Ghariblu. Analysis of wheeled mobile flexible manipulator dynamic motions with maximum load carrying capacities. *Robotics and Autonomous Systems*, 48(2):63–76, 2004.

Moharam Habibnejad Korayem, HN Rahimi, and A Nikoobin. Mathematical modeling and trajectory planning of mobile manipulators with flexible links and joints. *Applied Mathematical Modelling*, 36(7):3229–3244, 2012.

Signe Moe, Gianluca Antonelli, Andrew R Teel, Kristin Y Pettersen, and Johannes Schrimpf. Set-based tasks within the singularity-robust multiple task-priority inverse kinematics framework: General formulation, stability analysis, and experimental results. *Frontiers in Robotics and AI*, 3:16, 2016.

T. Moore and D. Stouch. A generalized extended kalman filter implementation for the robot operating system. In *Proceedings of the 13th International Conference on Intelligent Autonomous Systems (IAS-13)*. Springer, July 2014.

Yoshihiko Nakamura. *Advanced robotics: redundancy and optimization*. Addison-Wesley Longman Publishing Co., Inc., 1990.

Yoshihiko Nakamura, Hideo Hanafusa, and Tsuneo Yoshikawa. Task-priority based redundancy control of robot manipulators. *The International Journal of Robotics Research*, 6(2):3–15, 1987.

Evangelos Papadopoulos and Yves Gonthier. A framework for large-force task planning of mobile and redundant manipulators. *Journal of Robotic Systems*, 16(3):151–162, 1999.

John Schulman, Jonathan Ho, Alex X Lee, Ibrahim Awwal, Henry Bradlow, and Pieter Abbeel. Finding locally optimal, collision-free trajectories with sequential convex optimization. In *Robotics: science and systems*, volume 9, pages 1–10, 2013.

Lorenzo Sciavicco and Bruno Siciliano. *Modelling and control of robot manipulators*. Springer Science & Business Media, 2012.

Siciliano B Slotine. A general framework for managing multiple tasks in highly redundant robotic systems. In *proceeding of 5th International Conference on Advanced Robotics*, volume 2, pages 1211–1216, 1991.

Sebastian Thrun, Wolfram Burgard, and Dieter Fox. Probabilistic robotics. 2005. *CURRICULUM VITAE*, 2005.

JJ Uicker, J Denavit, and RS Hartenberg. An iterative method for the displacement analysis of spatial mechanisms. *Journal of Applied Mechanics*, 31(2):309–314, 1964.

Jianxin Xu, Wei Wang, and Yuanguang Sun. Two optimization algorithms for solving robotics inverse kinematics with redundancy. *Journal of Control Theory and Applications*, 8(2):166–175, 2010.

Yoshio Yamamoto and Xiaoping Yun. Coordinating locomotion and manipulation of a mobile manipulator. In *Decision and Control, 1992., Proceedings of the 31st IEEE Conference on*, pages 2643–2648. IEEE, 1992.

Appendix A

DH parameters

Link	d_i	θ_i	a_i	α_i
1	0	$\frac{\pi}{2}$	0	$\frac{\pi}{2}$
2	q_x	$\frac{\pi}{2}$	0	$\frac{\pi}{2}$
3	q_y	$\frac{\pi}{2}$	0	$\frac{\pi}{2}$
4	0	q_θ	0	0
5	0.653	0	0.27	0
6	0	$\frac{\pi}{2}$	0.01	0
7	0.1273	q_0	0	$\frac{\pi}{2}$
8	0	q_1	-0.612	0
9	0	q_2	-0.5723	0
10	0.163941	q_3	0	$\frac{\pi}{2}$
11	0.1157	q_4	0	$-\frac{\pi}{2}$
12	0.0922	q_5	0	0

Table A.1: Thing's DH parameters

Appendix B

Robot operating system

ROS is an open source software development tool for implementing robotics software. It provides the opportunity of hardware abstraction, low level device control, implementation of commonly used functionalities, messages between different processes and package management. It provides tools and libraries which utilize the opportunity of communicating between distributed computers, obtaining, writing and running code.

ROS has three different levels of concepts

- **The file system level**

Handles the main unit for a ROS system which is packages. A package may include data sets, ROS dependent libraries, configuration files etc. to define a ROS process. In ROS a process is denoted as a node.

- **The computation graph level**

Handles the communication of the peer to peer network of the system in which data is processed. Through the computation graph level, the different nodes can communicate with each other by messages. When a node is sending data it is said to be publishing a topic. The different nodes can then subscribe to this topic to get the information that is published.

- **The Community level**

ROS has a huge community which contains distribution of software installations, repositories and documentation of ROS. It also has a question and answer section with ROS related topics.

This community makes the process of learning the system considerably easier.

From Global to Local: Maintaining Accurate Mobile Manipulator State Estimates Over Long Trajectories

Abstract

Abstract.

Keywords: Keywords.

Naslov

Sažetak

Sažetak na hrvatskom jeziku.

Ključne riječi: Ključne riječi, odvojene zarezima.